Journal of Power Sources 202 (2012) 217–224

Contents lists available at SciVerse ScienceDirect

Journal of Power Sources

journal homepage: www.elsevier.com/locate/jpowsour

On the poisoning effect of O_2 and N_2 for the $Zr_{0.9}Ti_{0.1}V_2$ hydrogen storage alloy

T.B. Zhang*, X.W. Yang, J.S. Li, R. Hu, X.Y. Xue, H.Z. Fu

State Key Laboratory of Solidification Processing, Northwestern Polytechnical University, Xi'an 710072, PR China

ARTICLE INFO

Article history:
Received 2 June 2011
Received in revised form 1 December 2011
Accepted 2 December 2011
Available online 13 December 2011

Keywords:
Hydrogen absorption
Regeneration
Gaseous impurities
XPS
Poison

ABSTRACT

Homogeneously annealed $Zr_{0.9}Ti_{0.1}V_2$ samples are firstly exposed to contamination gases of O_2 and N_2 for 30, 60 and 180 s at the ambient temperature, respectively. Hydrogen absorption properties are examined after poisoning and regeneration. The compositions and valence in the surface and subsurface are investigated by X-ray photoelectron spectroscopy (XPS). The hydrogen absorption capacity of the alloy has been almost entirely degraded by the oxygen poisoning. After the regeneration, the oxygen-poisoned sample can hardly absorb hydrogen while the nitrogen-poisoned sample re-obtains the hydrogen absorption capacity with the value as 2.85 H A^{-1} (molar ratio of hydrogen to alloy). The activation temperature of the oxygen-poisoned sample is ~100 K higher than the value of the un-poisoned one. With the help of ion etching, it is found the thickness of the passivated surface layer of the oxygen-poisoned sample was ~58 nm. However, the thickness of the passivated surface layer of the un-poisoned sample is only ~36 nm. That is the reason why the oxygen-poisoned sample cannot renew the hydrogen absorption capacity under the same regeneration conditions as in the un-poisoned one.

1. Introduction

Hydrogen storage alloys are susceptible to surface contamination by reactive gases, which are crucial problems in practical applications [1–4]. Poisoning gases adsorbed on the surface of alloys can drastically decrease the hydrogen absorption rate by blocking the dissociation of the H_2 molecules. Even low impurity concentrations in the hydrogen gas can poison surface and destroy the hydrogenation performance [4]. It has been observed the hydrogen absorption kinetics of $LaNi_5$ is strongly influenced by the gaseous impurities including O_2, H_2O and CO [1,4,5]. In addition, the alloys poisoned by gaseous impurities cannot be easily reactivated and the particular reactivation cycles are always required [4]. In the investigations on the poisoning behavior of gaseous impurities, it is normally examined the effect of additives in the hydrogen gas on the reaction rate and the absorption capacity of storage alloys [1–3,5–7]. Research on the poisoning process and the corresponding poisoning mechanism will be valuable for the technical applications of hydrogen storage alloys. Exploring the alloys resistive to poison and searching of the efficient protective method have been the research focus during past decades [6,8,9].

Hydrogenation properties of Zr-based Laves phase alloys have been extensively investigated considering their potential applications in the storage and purification of hydrogen and its isotopes [10–15]. The Zr-based alloys have shown several preferable hydrogenation properties including high storage capacity, rapid kinetics and ease of activation [12,16]. But the hydrides of Zr-based alloys are too stable to be of practical significance [17]. In addition, the large hysteresis between hydrogenation and dehydrogenation make the alloys difficult to be used in practical applications [18,19]. Research efforts have been devoted to improve the shortcomings of Zr-based alloys by substitution of A or B site element in AB_2 phase by alloying elements [20]. The partial substitution of Zr by Ti has been proved to be an efficient way to improve the hydrogenation properties of Zr-based Laves phase alloys [13,16,21]. In our previous work $(Zr_{1-x}Ti_x)V_2$ $(0 \le x \le 1)$ alloys have been found to absorb/desorb hydrogen rapidly and preserve an acceptable reversibility [13,22,23]. Twin defects result from titanium substitution significantly improve hydrogen absorption kinetics and the decrease in hysteresis is observed in $(Zr_{1-x}Ti_x)V_2$ Laves phase alloys [13,22,23]. For the practical applications, the hydrogen storage capacity of Zr-based Laves phase alloys is inevitably affected by gaseous impurities which are always concerned in hydrogen storage alloys [1,4,5]. O_2 and N_2 gaseous impurities are of particular concern since they can be present with a small concentration in the hydrogen source or originate from atmospheric sources such as system leaks. The oxygen impurity is also of great importance in the activation processes as it can result from the oxygen-containing species such as carbon oxides and H_2O [3]. It has been reported the properties of

* Corresponding author. Tel.: +86 29 88491764; fax: +86 29 88460294.
E-mail address: tiebangzhang@nwpu.edu.cn (T.B. Zhang).

0378-7753/$ – see front matter © 2011 Elsevier B.V. All rights reserved.
doi:10.1016/j.jpowsour.2011.12.002

hydrogen storage alloys are always degraded by gaseous impurities [1,3–5]. However, the available literature is still insufficient to understand the poisoning mechanism of gaseous impurities on the hydrogen absorption properties of Zr-based Laves phase alloys.

In this contribution, a typical $(Zr_{1-x}Ti_x)V_2$ alloy with $x = 0.10$ was selected to investigate the poisoning effect of O_2 and N_2 gaseous impurities on the hydrogen absorption properties of Zr-based Laves phase alloys. The poisoning processes of $Zr_{0.9}Ti_{0.1}V_2$ alloy by O_2 and N_2 and the corresponding mechanism were investigated. Hydrogen absorption properties of regenerated alloys were evaluated after the contamination of gaseous impurities. The compositions and valence in the surface and sub-surface were analyzed with the help of X-ray photoelectron spectroscopy (XPS). The major influence factors of the re-activation are discussed as well. Correspondingly, the poisoning mechanism of Zr-based Laves phase alloys is proposed. The results will shed light on the practical applications of Zr-based hydrogen storage alloys.

2. Experimental procedures

The $Zr_{0.9}Ti_{0.1}V_2$ alloy was prepared by the magnetic induction levitation melting method under argon atmosphere in a water-cooled copper crucible. The purities of the raw materials zirconium, titanium, and vanadium were 99.4 wt.%, 99.8 wt.% and 99.5 wt.%, respectively. The alloy was homogeneously annealed at 1373 K for 100 h under the vacuum of 10^{-3} Pa. The experiments of pre-exposure and hydrogen absorption were conducted in an ultra high vacuum apparatus at the ambient temperature with a volume of 67 cm^3. The purities of O_2, N_2 and H_2 are 99.2, 99.5 and 99.99%, respectively.

Each test was performed by the following procedure. Firstly, a fresh sample was activated by conventional method and then exposed to a defined initial pressure (~1000 Pa) of contamination gas for 30, 60 and 180 s, respectively. After the poisoning treatment, the reactor was evacuated again and the sample was loaded in pure hydrogen. The reaction kinetics was evaluated from the pressure decrease in the reactor. The regeneration process was performed by the out-gassing method in vacuum at 823 K for 10 min. The samples with the diameter of Φ8 and the thickness around 1.0 mm were used in this work. The weight of samples exposed in N_2 and O_2 is 0.2073 and 0.1820 g, respectively. In order to maintain the initial condition, the sample was continuously used for the poisoning experiments after the same regenerating treatment. The absorbed hydrogen amount of the sample was determined by calculating the pressure variation during the reaction while maintaining constant temperature of the reaction chamber. The hydrogen content was calculated as the hydrogen-to-alloy mole ratio ($H A^{-1}$).

To characterize the surface and subsurface of the $Zr_{0.9}Ti_{0.1}V_2$ alloy before and after exposure to the gaseous impurities, the XPS experiment was performed in an ultra-high-vacuum chamber equipped with an XPS spectrometer ESCALAB 250 (multi-channel hemispherical energy analyzer) and a dual Al/Mg X-ray source using the Al Kα excitation (1486.6 eV, 300 W). The area of the ion etching is 4 mm^2 (2 mm × 2 mm). The parameters of the ion gun are: 2 kV beam, 2 μA sample current, depth by 2 nm per second. The base pressure of the chamber is 5.5×10^{-6} Pa. In each ion etching cycle, the XPS spectra were not recorded until the sample has been kept in a specific time. The binding energy (BE) scale was calibrated by measuring the carbon (C 1s, 284.6 eV) core level signal before and after the measurements.

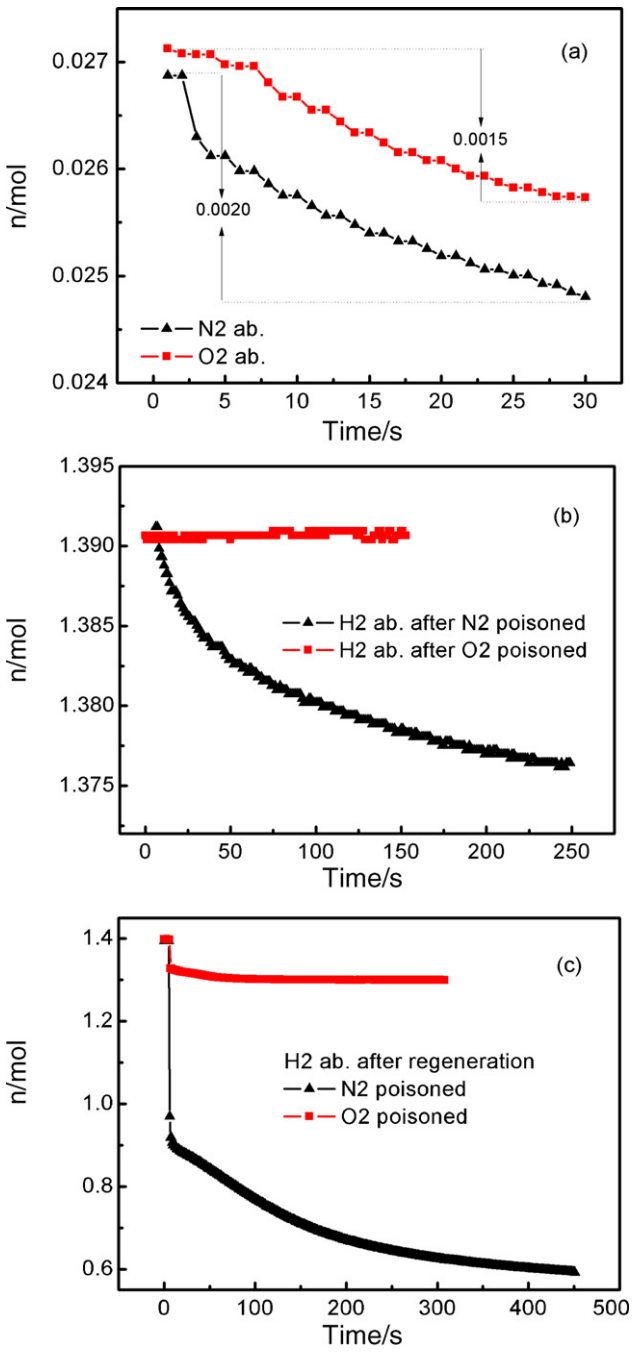

Fig. 1. The comparison of the alloys pre-exposed in the O_2 and N_2 for 30 s, and the hydrogen absorption properties of the regenerated samples. (a) Variations of absorbed gaseous impurities versus time, (b) the hydrogen storage amount versus time of the poisoned samples, and (c) the hydrogen storage amount versus time of the regenerated samples.

3. Results and discussion

3.1. Hydrogenation properties of the poisoned alloy

Fig. 1 shows *P–t* curves of the samples pre-exposed in the O_2 and N_2 for 30 s, and the poisoned samples before and after the regeneration. The system pressure decreases as the full activated sample exposed in the oxygen or nitrogen environment. The pressure decrease of the oxygen is about 55 Pa while the data of the nitrogen is around 77 Pa and the sample can rapidly absorb oxygen and nitrogen within 30 s. From Fig. 1a, the calculated amount

of absorbed O_2 and N_2 is 0.0015 and 0.0020 mol, respectively. According to our previous research, the maximum hydrogen storage capacity of a fully activated fresh $Zr_{0.9}Ti_{0.1}V_2$ alloy reaches as high as 3.90 H A^{-1} [22,23]. Hydrogenation properties of oxygen and nitrogen-poisoned samples were evaluated to examine the hydrogen absorption capacity of samples contaminated by gaseous impurities. Fig. 1b compares the hydrogen absorption pressure versus time (P–t) curves of the poisoned samples (y-axis has been changed as the amount of gas). The results indicate the poisoned sample loses almost the entire hydrogen absorption capacity. Meanwhile, the nitrogen-poisoned sample loses most of its hydrogen absorption capacity and only a few of capacity (0.25 H A^{-1}) can be reserved comparing with the data (3.90 H A^{-1}) of the fresh alloy. The oxygen almost destroys the hydrogenation storage capacity of the experimental Zr-based Laves phase alloy, while the nitrogen significantly decreases the value. The regeneration by a special designed procedure at the suitable temperature is always necessary to renew the hydrogen absorption capacity [5]. In this work, both gaseous impurity poisoned samples were regenerated in vacuum at 823 K for 10 min. Hydrogen absorption P–t curves of the regenerated samples are displayed in Fig. 1c. After the same regeneration progress, the oxygen-poisoned sample absorbs only a little hydrogen with the value of 0.64 H A^{-1}, while the nitrogen-poisoned sample renews the hydrogen absorption capacity with the value as high as 2.85 H A^{-1} (molar ratio of hydrogen to alloy). The nitrogen-poisoned sample obtains most of the hydrogen absorbing capacity with the help of the regeneration process, but the oxygen-poisoned one hardly absorbs hydrogen even it has been regenerated at the same condition.

The compared data of pre-exposure in the O_2 and N_2 for 60 s are displayed in Fig. 2a. The decrease of pressure in the oxygen and nitrogen is about 25 Pa and 30 Pa, and the calculated amount of the absorbed O_2 and N_2 is 0.0007 and 0.0008 mol, respectively. As the hydrogen absorption capacity has been almost disappeared after poisoned by the oxygen or nitrogen for 30 s, the hydrogen absorption P–t curves are not necessary to measure for the samples pre-exposed in gases (O_2 or N_2) for 60 s. Both poisoned samples were regenerated in vacuum at 823 K for 10 min after the pre-exposure. Fig. 2b describes the hydrogen absorption P–t curves for the regenerated samples. After the regeneration, the nitrogen-poisoned sample renews the hydrogen absorption capacity with the value of 2.25 H A^{-1}. However, the oxygen-poisoned sample only re-obtains the absorption capacity of 0.27 H A^{-1}.

As the pre-exposure time is prolonged to 180 s, the system pressure for O_2 and N_2 poisoned samples is decreased (see Fig. 3a) and the values for O_2 and N_2 poisoned samples are 15 and 22 Pa, respectively. The corresponding absorbing or adsorbing amount of O_2 and N_2 is 0.0004 and 0.0006, respectively. After the regeneration, the nitrogen-poisoned sample re-obtains the hydrogenation capacity with the value of 1.27 H A^{-1} (see Fig. 3b). However, the oxygen-poisoned sample preserves the hydrogen absorption capacity of around 0.27 H A^{-1} after the same regeneration process. These three compared data (from Figs. 1–3) demonstrate that the oxygen plays an essential role in poisoning $Zr_{0.9}Ti_{0.1}V_2$. The poisoning mechanisms are probably different between oxygen and nitrogen. When the sample is exposed in the oxygen, O_2 molecules are firstly absorbed by chemisorption. Various oxides of metallic are always formed during the poisoning process as have been observed in oxygen-poisoned hydrogen storage alloys [9,24]. The hydrogen diffusion is blocked by the oxide layer of the O_2 poisoned sample. As a result, the O_2 poisoned sample does not absorb hydrogen at all as shown in Fig. 1b. As the N—N bond is steady at room temperature, the nitrogen molecule is not easy to release or capture electron. It can be believed N_2 molecules are probably adsorbed by physisorption when the sample is exposed in the nitrogen. During the regeneration, the adsorbed N_2 is released by the process

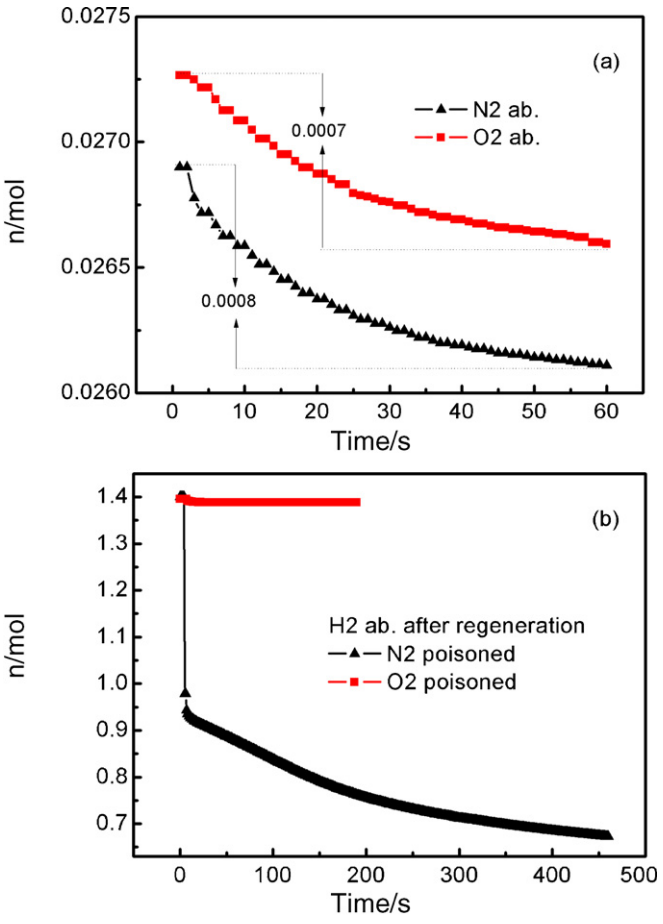

Fig. 2. The comparison of the alloys pre-exposed in the O_2 and N_2 for 60 s, and the hydrogen absorption properties of the regenerated samples. (a) Variations of absorbed gaseous impurities versus time and (b) the hydrogen storage amount versus time of the regenerated samples.

of desorption. Then the fresh surfaces could be obtained and the hydrogen absorbing capacity can be regenerated. However, the absorbed oxygen atoms could diffuse into the inside of the alloy during the activation. The newly activated surfaces are poisoned again at once in the environment with oxygen impurities [4]. As a result, the fairly thick oxide film is formed and the activity of surface sites is reduced inevitably. The oxidation layer do greatly block the hydrogen diffusion to the inside of the alloy [3].

Furthermore, the thermal activation process of the un-poisoned sample and the re-activation process of the oxygen-poisoned one have been investigated. The results are illustrated in Fig. 4. From Fig. 4a, the system pressure increases gradually during the calefactive process due to the expending of hydrogen under the heat. As the temperature reaches 600 K, the significant decrease system pressure gives the evidence that the un-poisoned sample has been activated at the experimental temperature. The hydrogen absorption process cannot be completed until the temperature higher than 620 K. The pressure in the system gradually increases again for the expending of hydrogen. For the oxygen-poisoned sample, it is difficult to be re-activated at the same calefactive process and hydrogen pressure. The re-activation process is shown in Fig. 4b. The system pressure does not decrease until the temperature reaches 703 K.

3.2. Poisoning mechanism and regeneration

To explain the above mentioned difference, the ion etching method in XPS investigation has been performed. The

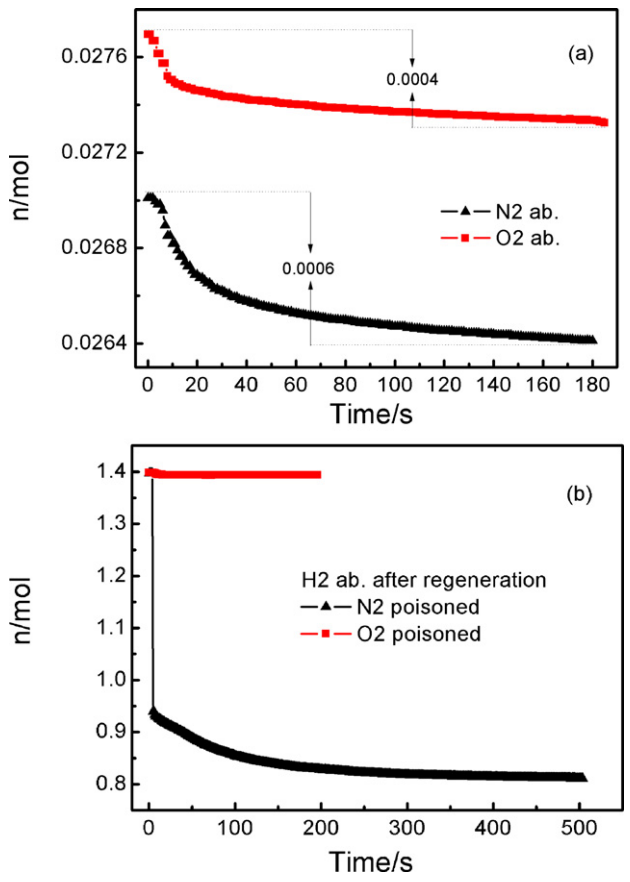

Fig. 3. The comparison of the alloys pre-exposed in the O_2 and N_2 for 180 s, and the hydrogen absorption properties of the regenerated samples. (a) Variations of absorbed gaseous impurities versus time and (b) the hydrogen storage amount versus time of the regenerated samples.

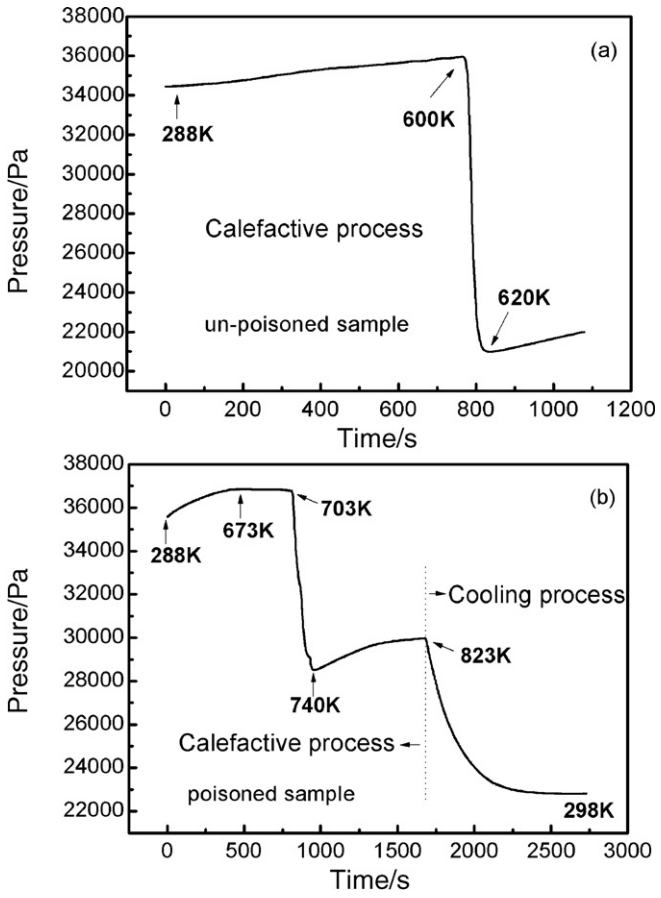

Fig. 4. The thermal activation process of the un-poisoned sample (a) and the re-activation process of the oxygen-poisoned sample (b), both in the hydrogen.

compositions in the surface and sub-surface of the $Zr_{0.9}Ti_{0.1}V_2$ alloy before and after the contamination by gaseous impurities are investigated. The surface composition can be calculated from Zr 3d, Ti 2p, V 2p, O 1s and C 1s peaks areas using empirically determined sensitive factors after each ion etching process. A series of Zr 3d spectra of the un-poisoned sample ion etched at various times are plotted in Fig. 5a. The appearance of the main Zr 3d spectra peaks in the initial surface can be attributed to the oxide ZrO_2 at binding energy (BE) of ($3d_{5/2}$) 182.5 eV and ($3d_{3/2}$) 185.0 eV, sub-oxide ZrO (180.6 eV) and metallic Zr (178.9 eV) according to Ref. [23,25,26]. The intensity of the ZrO_2 oxide is the dominant among the three compositions. After 60 s ion etching, the intensity of the ZrO_2 peak decreases while the intensity of the metallic Zr peak increases together with a peak at 180.6 eV which can be associated with the low valence zirconium sub-oxide and/or zirconium carbide [23,24]. As the ion etching time reaches 180 s, the intensities of the oxide and sub-oxide peaks decrease significantly. However, the metallic zirconium peak has been broadened in addition to the intensity increase. It suggests that the zirconium oxide has been eliminated after 180 s ion etching. The depth of the oxide layer of the un-poisoned alloy is no more than 36 nm judging from XPS analysis. Fig. 5b shows a series of Ti 2p XPS spectra of $Zr_{0.9}Ti_{0.1}V_2$ alloy surface/sub-surface at various ion-etching conditions. The Ti 2p spectrum of the initial surface exhibits a dominant peak corresponding to the titanium oxide at a BE of 459 eV ($\Delta = 5.7$) [9]. After 60 and 180 s ion etching, the compositions in the sub-surface have been entirely changed. The metallic titanium (Ti $2p_{3/2}$) at a BE of 454 eV ($\Delta = 6.1$) [9] becomes the dominant composition. The peak at 460 eV corresponds to the metallic titanium of Ti $2p_{1/2}$. These results indicate that the oxidized titanium in the surface layer has been entirely deoxidized to metallic Ti during the ion etching process.

Similar to the results in the published literature [24,25], the V 2p spectra of the initial surface exhibit several elementary peaks which can be attributed to different V^{n+} states representing a mixed valence vanadium oxides (see Fig. 5c). The V_2O_5 $2p_{3/2}$ peak is most intensive on the initial surface, while other peaks can be ascribed to the vanadium metallic state (512.4 eV) and vanadium sub-oxide state or vanadium carbide state (514.5 eV), respectively [23]. The V^{5+} peak (V_2O_5 at a BE of 517.2 eV) does not exist in the XPS spectra after the ion etching, suggesting that the V_2O_5 $2p_{3/2}$ peak has disappeared. The V 2p spectra of the $Zr_{0.9}Ti_{0.1}V_2$ alloy can be ascribed to vanadium metallic state peak as the layer of oxides have been removed during the ion etching process. Fig. 5d shows the C 1s XPS spectra for various ion etching times. The results indicate that the compositions in the surface and sub-surface are entirely different. The C 1s spectra decompose into two component peaks during the etching process. The XPS peaks represent C in various chemical states. Before the ion etching, the C 1s spectrum peak at a BE of ~285 eV can be attributed to the hydrocarbons [27]. Surface hydrocarbons have been entirely eliminated after a 60 s ion etching. The spectrum peak preserves a remarkable chemical shift to the lower binding energy typical for carbide species. The position of the carbide related peak (282.6 eV) implies that most of the carbon atoms are bonded to vanadium or titanium [23,28]. From Fig. 5e, the intensity decrease of the O 1s peak after the ion etching corresponds to the increase of the metallic Zr, Ti and V in the sample's sub-surface. The O 1s spectrum includes two main elementary peaks: around 531.1 eV corresponds to a metal oxide and 532.9 eV commonly refers to the hydroxyl group [24,29]. The intensity decrease

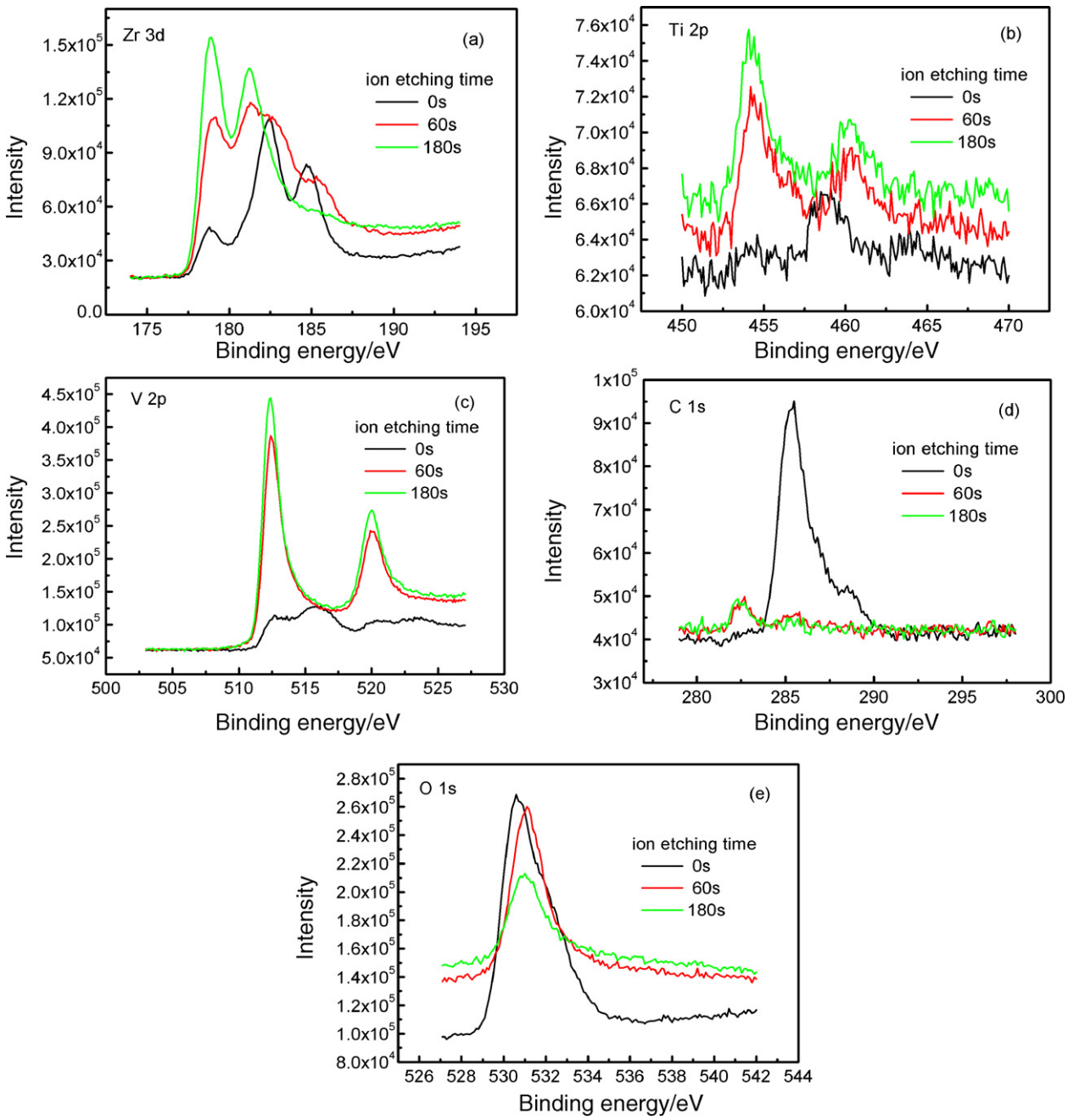

Fig. 5. XPS spectra of the surface and sub-surface for the un-poisoned $Zr_{0.9}Ti_{0.1}V_2$ alloy. (a) Zr 3d, (b) Ti 2p, (c) V 2p, (d) C 1s, and (e) O 1s.

of the metal oxide and OH group peaks are observed after the ion etching process, which is in agreement with the reduction of the metal oxide and sub-oxide related intensity in Zr 3d, V 2p and Ti 2p spectra [24,30].

In comparison with the un-poisoned sample, the poisoned sample preserves a much thicker oxide layer on the alloy surface and the evidence can be found in Fig. 6. From Fig. 6a, the zirconium oxide and/or zirconium carbide is still observed after the 180 s ion etching process even though the etching time is prolonged to 290 s. The surface investigations reveal the oxygen contaminated alloy in which the zirconium oxide can be eliminated only after 180 s ion etching is different from the un-poisoned one. The depth of the oxide layer in the oxygen-poisoned sample is not less than 58 nm. From Fig. 6b, Ti peaks exhibit the dominant oxide at a BE of 459 eV and metallic characteristic at 454 eV. With the effect of the iron etching, obvious metallic peaks of titanium at 454 eV and 460 eV are observed in the samples ion etched at various times. In case of the vanadium spectra in Fig. 6c, metallic peaks at 512.9 eV and vanadium sub-oxide state at 516.0 eV of the oxygen-poisoned sample are observed [23]. After the ion etching, the V 2p spectra of the alloy can be ascribed to vanadium metallic state peaks as observed in the un-poisoned sample due to the removal of the oxide layers during the ion etching process. Titanium and vanadium oxides can be significantly reduced after 180 s ion etching on the surface of oxygen-poisoned alloy as shown in Fig. 6b and c. Judging from the C 1s spectrum peak (~285 eV) in Fig. 6d, the hydrocarbons on the surface of the oxygen-poisoned alloy is still prevalent even

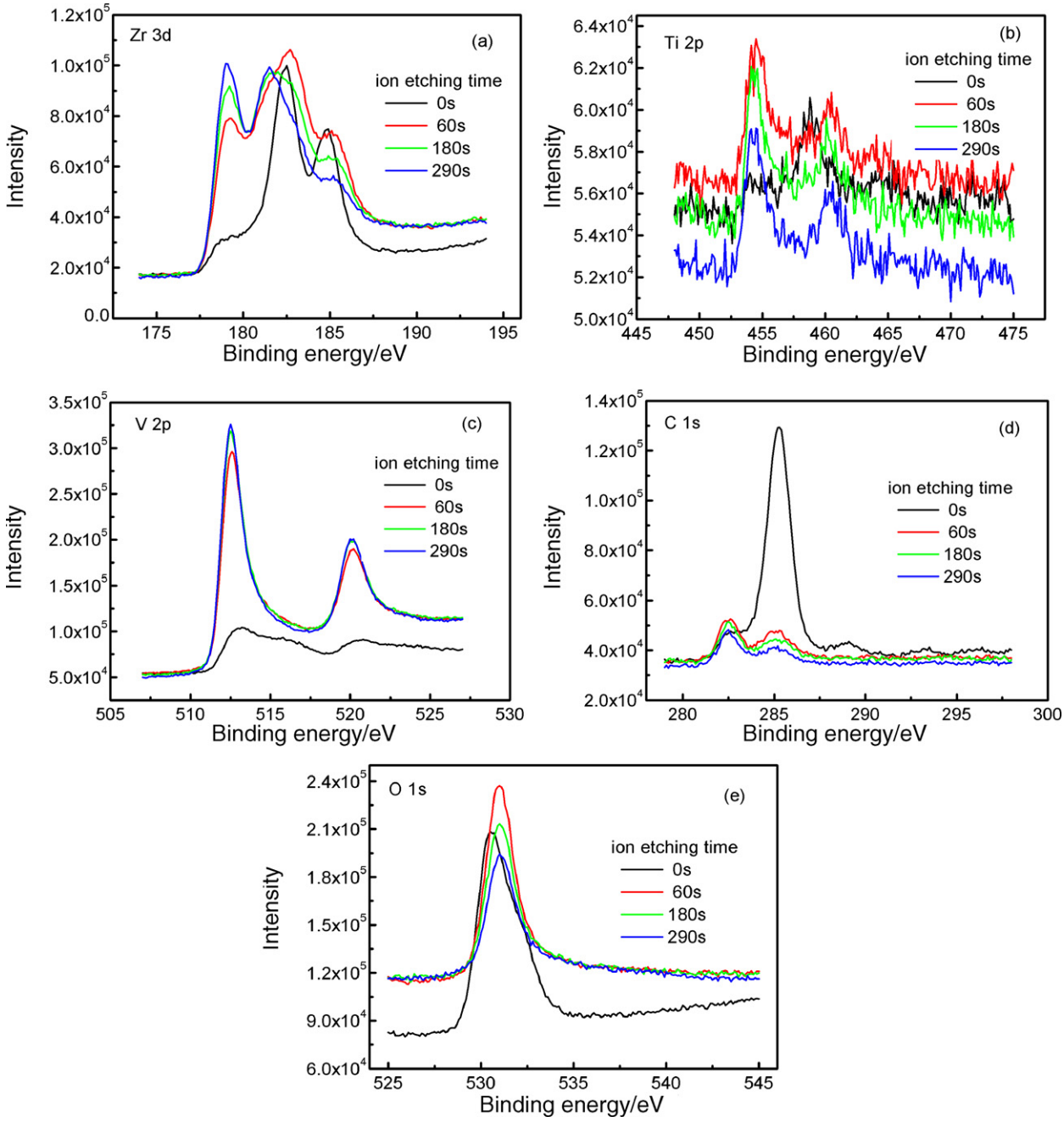

Fig. 6. XPS spectra of the surface and sub-surface for the oxygen-poisoned $Zr_{0.9}Ti_{0.1}V_2$ alloy. (a) Zr 3d, (b) Ti 2p, (c) V 2p, (d) C 1s, and (e) O 1s.

with the long time ion etching process. In addition, the carbide vanadium or titanium at 282.6 eV is also observed in each sample etched at various times. Fig. 6d exhibits the surface hydrocarbons have also been entirely eliminated after 60 s ion etching. However, the intensity of the O 1s spectrum in Fig. 6e does not decrease obviously even after a 290 s ion etching process. The results agree well with the aforementioned analysis that zirconium oxide existing in the sub-surface. Comparing the oxygen-poisoned sample with the un-poisoned one, the main factor determining the activation property can be mainly attributed to the zirconium oxide as the Zr—O bond is difficult to be destroyed. During the first thermal activation process, oxygen atoms probably diffuse into the sub-surface as the Zr—O bond is easy to be recombined. When the activated sample is pre-exposed in O_2, the new oxides will be formed and the surface will be covered by the passivated layer. As a result, the oxides are not easy to be reduced upon the thermal activation process and the oxygen-poisoned alloy always requires higher temperature and longer time to be reactivated. Fig. 7 illustrates XPS spectra of the surface and sub-surface for the alloy pre-exposed in N_2. It is necessary to note that a small quantity of sub-oxides of zirconium and titanium are observed in the nitrogen-poisoned sample due to the possible air exposure during the preparation and transition of the alloy. After the ion etching process, the hydrocarbons in the nitrogen-poisoned alloy can be almost removed as observed in the un-poisoned. The significant reduction of hydrocarbons on the etched surface of nitrogen-poisoned alloy during the ion

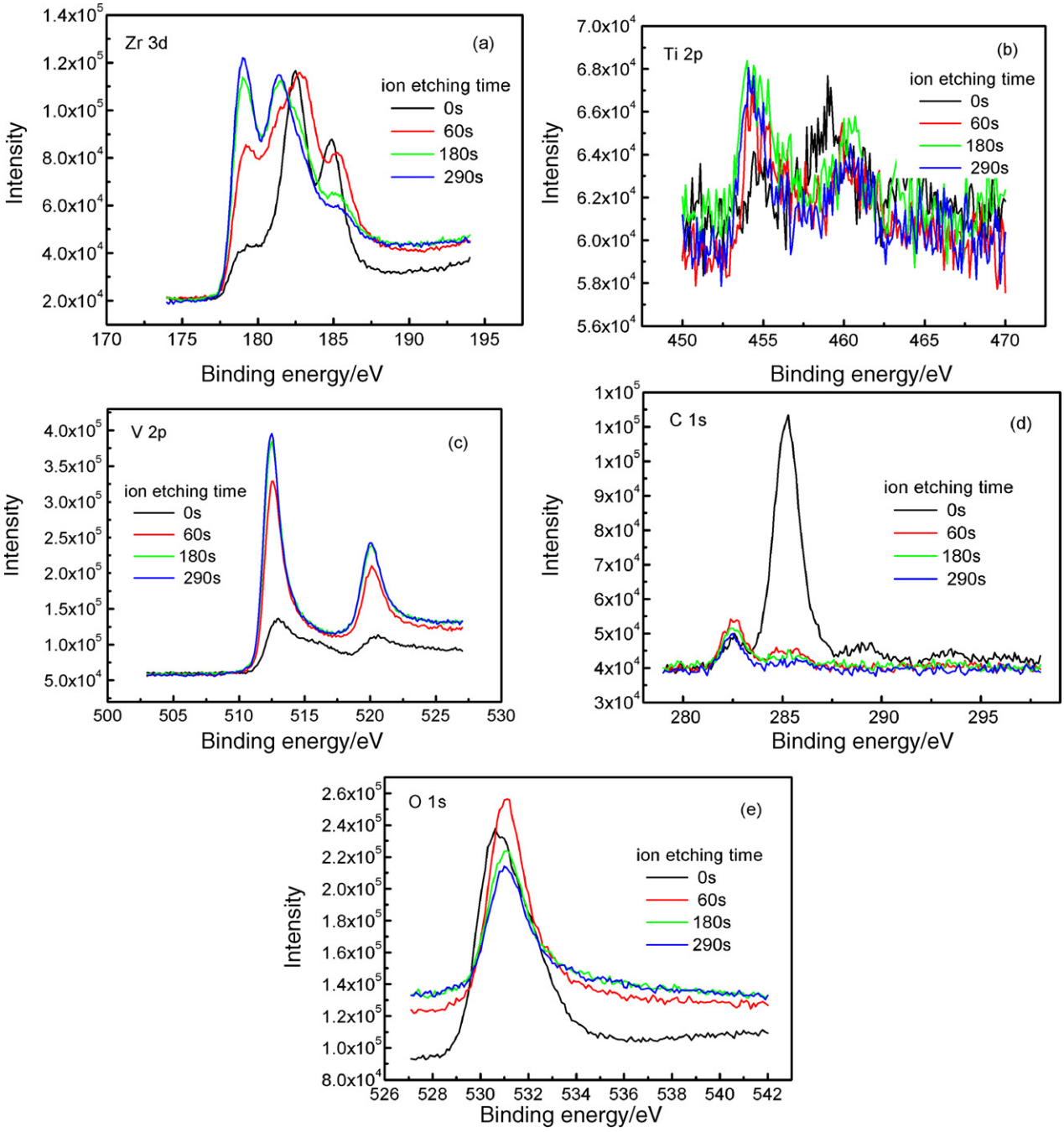

Fig. 7. XPS spectra of the surface and sub-surface for the nitrogen-poisoned $Zr_{0.9}Ti_{0.1}V_2$ alloy. (a) Zr 3d, (b) Ti 2p, (c) V 2p, (d) C 1s, and (e) O 1s.

etching process partially accounts for the easy activation during the regeneration process comparing with that of the oxygen-poisoned one. No nitride is identified in the XPS spectra of nitrogen-poisoned alloy, which gives the evidence that N_2 molecules are adsorbed by the physisorption. During the regeneration, the adsorbed N_2 is easy to be released and the hydrogen storage capacity of the nitrogen-poisoned sample can be re-obtained conveniently.

From the aforementioned analyses, the regenerated hydrogen storage capacity of the oxygen-poisoned alloy is much smaller comparing with that of the nitrogen-poisoned one. That is to say the alloy pre-exposed in oxygen can be hardly activated at the same regenerating process as the nitrogen-poisoned sample. It is necessary to investigate whether the oxygen-poisoned alloy can be regenerated to absorb proper hydrogen or not and the corresponding required regenerating conditions considering the technical applications of Zr-based Lave phase alloys. The regeneration time of the experimental alloys was prolonged to 1 h at 823 K. After the out-gassing process, the hydrogen absorption curve as a function of time measured at room temperature is shown in Fig. 8. The hydrogen absorption curve in Fig. 8 indicates the pressure decreases significantly versus time and the absorbed amount of hydrogen is around 0.70 mol. The regenerated sample preserves acceptable hydrogen absorption kinetics and

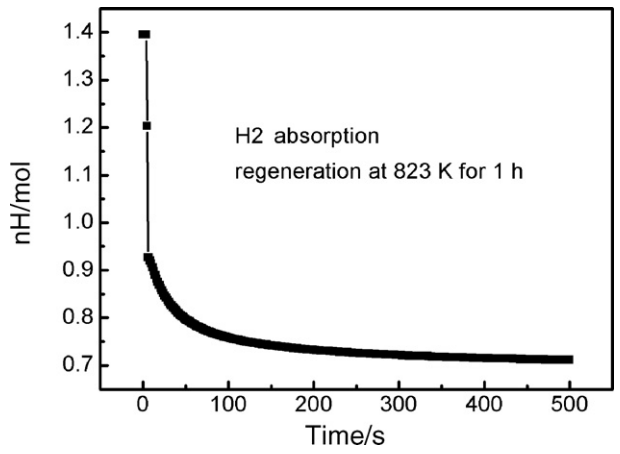

Fig. 8. The hydrogen storage amount versus time at ambient temperature for the oxygen-poisoned $Zr_{0.9}Ti_{0.1}V_2$ alloy regenerated at 823 K for 1 h.

the hydrogenation capacity reaches as high as 2.756 H A^{-1}, which demonstrates oxygen-poisoned sample can also be regenerated at a special designed rigorous activation process.

4. Conclusions

In this work, effect of gaseous impurities on the hydrogenation properties of Zr-based Laves phase alloy and the corresponding mechanism were investigated. The compositions and valence in the surface and sub-surface were analyzed by X-ray photoelectron spectroscopy (XPS). The conclusions are as follows: hydrogen absorption capacity of oxygen-poisoned sample has been almost disappeared. Under the same regeneration progress, the oxygen-poisoned sample can hardly absorb hydrogen while the nitrogen-poisoned one can renew the hydrogen absorption capacity with the value is 2.85 H A^{-1}. The activation temperature of the oxygen-poisoned sample is 100 K higher than the value of the un-poisoned one. It can be found that the thickness of the passivated surface layer for the oxygen-poisoned sample is higher than 58 nm while the data of the un-poisoned one is only 36 nm. The thick oxide film and hydrocarbons on the surface inevitably block the hydrogen diffusion to the inside of the alloy. That is the reason why the oxygen-poisoned sample cannot renew the hydrogen absorption capacity under the same regeneration conditions. The oxygen-poisoned sample requires much more time during the regeneration than nitrogen-poisoned one at the same temperature. The composition tailoring and surface condition optimizing are necessary for the hydrogen storage alloys with the specific poisoning resistance to prevent the formation of the barrier layer and favor the hydrogen diffusion.

Acknowledgements

This work was financially supported by State Key Laboratory of Solidification Processing (NWPU) (70-QP-2010 and 38-TP-2009) and the Research Foundation of NWPU (R0217). The Program of Introducing Talents of Discipline in the Project of Advanced Materials and their Forming Technology (B08040) is also acknowledged.

References

[1] F.R. Block, H.J. Bahs, J. Less-Common Met. 89 (1983) 77–84.
[2] F.G. Eisenberg, P.D. Goodell, J. Less-Common Met. 89 (1983) 55–62.
[3] P.D. Goodell, J. Less-Common Met. 89 (1983) 45–54.
[4] F. Schweppe, M. Martin, E. Fromm, J. Alloys Compd. 253–254 (1997) 511–514.
[5] G.D. Sandrock, P.D. Goodell, J. Less-Common Met. 73 (1980) 161–168.
[6] G. Sang, X.J. Luo, Q.A. Li, K.P. Yan, M.J. Tu, Y.G. Chen, N. Li, Chin. J. Rare Met. 25 (2001) 178–180.
[7] G. Sang, Y.G. Chen, M.J. Tu, M.G. Han, J. Funct. Mater. 30 (1999) 137–140.
[8] M. Hara, Y. Hatano, T. Abe, K. Watanabe, T. Naitoh, S. Ikeno, Y. Honda, J. Nucl. Mater. 320 (2003) 265–271.
[9] F. Sutara, N. Tsud, K. Veltruská, V. Matolín, Vacuum 61 (2001) 135–139.
[10] M. Kandavel, V.V. Bhat, A. Rougier, L. Aymard, G.A. Nazri, J.M. Tarascon, Int. J. Hydrogen Energy 33 (2008) 3754–3761.
[11] X.-Y. Cui, Q. Li, K.-C. Chou, S.-L. Chen, G.-W. Lin, K.-D. Xu, Intermetallics 16 (2008) 662–667.
[12] D.J. Davidson, O.N. Srivastava, Int. J. Hydrogen Energy 26 (2001) 219–223.
[13] X.W. Yang, T.B. Zhang, R. Hu, J.S. Li, X.Y. Xue, H.Z. Fu, Int. J. Hydrogen Energy 35 (2010) 11981–11985.
[14] A.L.M. Reddy, S. Ramaprabhu, J. Alloys Compd. 460 (2008) 268–271.
[15] J. Cao, X. Gao, D. Lin, X. Zhou, H. Yuan, D. Song, P. Sen, J. Power Sources 93 (2001) 141–144.
[16] J.-M. Park, J.-Y. Lee, J. Alloys Compd. 182 (1992) 43–54.
[17] A. Jain, R.K. Jain, S. Agarwal, I.P. Jain, Int. J. Hydrogen Energy 32 (2007) 2445–2449.
[18] M. Jurczyk, W. Rajewski, G. Wójcik, W. Majchrzycki, J. Alloys Compd. 285 (1999) 250–254.
[19] X.W. Yang, J.S. Li, T.B. Zhang, R. Hu, X.Y. Xue, H.Z. Fu, Int. J. Hydrogen Energy 36 (2011) 9318–9323.
[20] N. Mani, R. Sivakumar, S. Ramaprabhu, J. Alloys Compd. 337 (2002) 148–154.
[21] G.P. Li, N. Nishimiya, H. Satoh, N. Kamegashira, J. Alloys Compd. 393 (2005) 231–238.
[22] X.F. Wang, R. Hu, X.Y. Xue, X.W. Yang, T.B. Zhang, J.S. Li, Rare Met. Mater. Eng. 40 (2011) 487–490.
[23] X.W. Yang, J.S. Li, T.B. Zhang, R. Hu, X.Y. Xue, X.F. Wang, H.Z. Fu, Solid State Commun. 151 (2011) 842–845.
[24] F. Sutara, I. Matolínová, T. Skála, K. Masek, V. Matolín, Vacuum 74 (2004) 305–309.
[25] V. Matolin, J. Drbohlav, K. Maek, Vacuum 71 (2003) 317–322.
[26] S. Sinha, S. Badrinarayanan, A.P.B. Sinha, J. Less-Common Met. 125 (1986) 85–95.
[27] S. Fabík, V. Cháb, V. Dudr, K. Masek, K.C. Prince, F. Sutara, K. Veltruská, N. Tsud, M. Vondrácek, V. Matolín, Surf. Sci. 566–568 (2004) 1246–1249.
[28] K. Masek, F. Sutara, T. Skala, J. Drbohlav, K. Veltruska, V. Matolin, J. Vac. Sci. Technol. A: Vac. Surf. Films 21 (2003) 797–805.
[29] V. Matolín, K. Masek, I. Matolínová, T. Skála, K. Veltruská, Appl. Surf. Sci. 235 (2004) 202–206.
[30] C.-C. Li, J.-L. Huang, R.-J. Lin, C.-H. Chen, D.-F. Lii, Thin Solid Films 515 (2006) 1121–1125.